International Journal of Modern Physics C
(2021) 2150072 (17 pages)

DOI: 10.1142/S0129183121500728

Analysis of Buongiorno's nanofluid model in marangoni convective flow with gyrotactic microorganism and activation energy

M. Ijaz Khan[*], Yu-Ming Chu[†,‡,¶], Faris Alzahrani[§] and Aatef Hobiny[§]

[*]*Department of Mathematics and Statistics*
Riphah International University
I-14, Islamabad 44000, Pakistan

[†]*Department of Mathematics, Huzhou University*
Huzhou 313000, P. R. China

[‡]*Hunan Provincial Key Laboratory of Mathematical Modeling and Analysis in Engineering*
Changsha University of Science & Technology
Changsha 410114, P. R. China

[§]*Nonlinear Analysis and Applied Mathematics (NAAM)-Research Group*
Department of Mathematics
Faculty of Sciences, King Abdulaziz University
P.O. Box 80203, Jeddah 21589 Saudi Arabia
[¶]*chuyuming@zjhu.edu.cn*

Please check that title, author's names, affiliations & keywords are correct.

Received 3 January 2021
Accepted 12 January 2021
Published

This communication is to analyze the Marangoni convection MHD flow of nanofluid. Marangoni convection is very useful physical phenomena in presence of microgravity conditions which is generated by gradient of surface tension at interface. We have also studied the swimming of migratory gyrotactic microorganisms in nanofluid. Flow is due to rotation of disk. Heat and mass transfer equations are examined in detail in the presence of heat source sink and Joule heating. Nonlinear mixed convection effect is inserted in momentum equation. Appropriate transformations are applied to find system of equation. HAM technique is used for convergence of equations. Radial and axial velocities, concentration, temperature, motile microorganism profile, Nusselt number and Sherwood number are sketched against important parameters. Marangoni ratio parameter and Marangoni number are increasing functions of axial and radial velocities. Temperature rises for Marangoni number and heat source sink parameter. Activation energy and chemical reaction rate parameter have opposite impact on concentration profile. Motile density profile decays via Peclet number and Schmidt number. Magnitude of Nusselt number enhances via Marangoni ratio parameter.

Keywords: Rotating disk; Marangoni convection; nanofluid; gyrotactic microorganism; heat source sink; activation energy; MHD; Joule heating; nonlinear mixed convection.

Please indicate corresponding author.

Nomenclature

$(u, w)\left[\frac{L}{t}\right]$	Velocity vector
$(r, \vartheta, z)[L]$	Cylindrical coordinates
$\nu\left[\frac{L^2}{t}\right], g\left[\frac{L}{t^2}\right]$	Kinematic viscosity, gravity
Q, Ec	Exponential space dependent heat source parameter
M, λ	Magnetic parameter, mixed convection
β_t, β_c	Nonlinear thermal and solution convection parameters
$\rho\left[\frac{Mass}{L^3}\right], \beta_1\left[\frac{1}{K}\right]$	Density, linear thermal expansion coefficient
$\beta_2\left[\frac{1}{K^2}\right]$	Nonlinear thermal expansion coefficient
$\beta_3[1], \beta_4[1]$	Linear and nonlinear solutal expansion coefficient
$(T, T_0, T_\infty)[K]$	Temperature of fluid, temperature at disk, ambient temperature
$N^*, \Pr$	Ratio of buoyancy to viscous forces parameter
$C_\infty[1], Lb$	Ambient Concentration, bioconvection Lewis number
$Q_t[1]$	Thermal dependent heat source parameter
$(C, C_0)[1]$	Concentration of fluid, Concentration at disk
$(N, N_0, N_\infty)\left[\frac{M}{L^3}\right]$	Density of fluid, density at disk, ambient density
$k\left[\frac{ML}{t^3K}\right], c_p\left[\frac{L^2}{t^2K}\right]$	Thermal conductivity, specific heat
$D_B\left[\frac{L^2}{t}\right], D_T\left[\frac{L^2}{t}\right]$	Brownian and thermophoretic diffusion coefficient
Nt, Nb	Thermophoresis and Brownian motion parameter
Sc, k_1	Schmidt number, chemical reaction rate parameter
δ, n_1	Temperature ratio parameter, fitted rate constant
n, Ω	Exponential index, density difference parameter
$Q_0\left[\frac{M}{t^3LK}\right]$	Exponential heat source coefficient
$B_0\left[\frac{M}{t^2 Ampere}\right]$	Magnetic field strength
$k_r\left[\frac{1}{\sqrt{t}}\right], n_1$	Chemical reaction rate
E_1, Pe	Activation energy coefficient, Peclet number
$\Omega_1\left[\frac{1}{t}\right], Ma$	Rotation frequency, Marangoni number
$r, Q_l\left[\frac{M}{t^3LK}\right]$	Thermal-based heat source
E_a	Activation energy parameter
$b[L]$	Chemotaxis constant
$D_n\left[\frac{L^2}{t}\right]$	Diffusivity of microorganisms
$\sigma\left[\frac{M}{t^2}\right], \mu\left[\frac{M}{Lt}\right]$	Surface tension, dynamic viscosity
Sh_x	Sherwood number
Nu_x	Nusselt number
Re_x	Reynolds number
$\sigma_0\left[\frac{M}{t^2}\right]$	Positive constants
$W_c\left[\frac{L}{t}\right]$	Maximum speed of swimming cell
$\sigma^*\left[\frac{t^3 Ampere^2}{L^3M}\right]$	Electrical conductivity

AQ: Please check short title running head.

$\gamma_T\left[\frac{M}{t^2K}\right], \gamma_C$	Constants
κ	Boltzmann constant

1. Introduction

Thermal and concentration distribution is the main cause of the appearance of Marangoni convective transport. Marangoni convection has wide range of its application in industries especially in crystal growth, welding, etc. surface tension has an important role in many engineering fields like in food industry, chemical industry and in electronic devices as well. Mizev and Trofimenko[1] examine the marangoni flow and its applications in process industry. Mahanthesh *et al.*[2] worked on Marangoni convection of Casson fluid with heat source effect. Lin *et al.*[3] studied the heat transfer in the boundary layer; the parameters which he studied are magnetic field and thermal conductivity. Surface tension is treated as a nonlinear function. The efficiency of evaporators can be increased by using micro structured surfaces is studied by Fujita,[4] Roisman and Stephan.[5,6] Surface tension decreases by increasing the temperature. Lin and Zheng[7] studied the Marangoni convection in copper water nanofluid with two phase model. Xu and Zebib[8] studied that these flows have an oscillatory behavior and they produce hydrothermal waves. Colinet *et al.*[9] and Nepomnyashchy *et al.*[10] studied that this flow is responsible for convective flows in the films, so they studied the transition between different patterns of convective flows.

Nanoparticles are the particles that are nanometer in size. They are colloidal solutions in the base fluid. They are typically used in nanofluids which are made up of copper, silver, etc. or nonmetals like graphite the base fluids that are used are convective fluids like glycol, water, etc. The type of base fluid depends on the application for which it is used. Nanofluids have wide range of applications in cancer treatment and in engineering industries as well. Nanofluids are very stable, viscous and they have good dispersing and wetting properties on the solid surfaces. The diameter of nanoparticles are between 1 nm and 100 nm. Choi[11] studied that the nanofluids have just 5% of nanoparticles of the total volume for effective heat transfer. Nanofluids have large applications in many industries especially in nuclear industry, etc. Gorla *et al.*[12] studied the heat transfer in nanofluids on a stretching sheet. Fakour *et al.*[13] studied the heat transfer in nanofluid flow in magnetic field. Makinde and Aziz[14] used RK method to study the flow of boundary layer on the stretching surface with convective boundary conditions. Mustafa *et al.*[15] studied the homotopy analysis method to study the boundary layer flow on a stretching sheet. Hamad *et al.*[16] used RK method to study the nanofluids over a nonlinear stretching surface. Bachok *et al.*[17] studied the boundary layer flow on stretching surface and heat transfer on it. Zaimi *et al.*[18] did the similar research on the stretching surface in nanofluids. Aman *et al.*[19] studied the two-dimensional flow on the linear stretching surface in the presence of magnetic field and the base fluid is viscous and incompressible. In his research work, he converted nonlinear differential equation to ODE by using shooting method. Uddin *et al.*[20] studied the analysis of 2D viscous convective boundary layer flow from a heated permeable vertical surface in the presence of chemical reaction. Uddin *et al.*[21] studied the 2D MHD flow of a conducting nanofluids from stretching surfaces in a quiescent fluid. Uddin *et al.*[22] studied the 2D, steady and laminar flow of nanofluids on porous surface in the presence of thermal radiations both numerically and theoretically. Some more advance work regarding this field can be seen through Refs. 23–33.

The purpose of this paper is to analyze the Marangoni convection flow of nanofluid over a rotating disk with gyrotactic microorganisms. In best of my knowledge, no work is done previously related to Marangoni convection with gyrotactic microorganisms and nanofluid. Also, additional effects of exponential space dependent heat source, activation energy, Joule heating, MHD and nonlinear mixed convection are studied. So, the purpose is to fill this void. HAM technique is used to find convergent solution. Impact of pertinent parameters on characteristics of fluid are shown graphically.

2. Mathematical Modeling

Here, we consider the incompressible steady flow of Marangoni convective fluid flow with nanofluid and gyrotactic microorganisms. We have also studied the swimming of migratory gyrotactic microorganisms in nanofluid. Flow is due to rotation of disk. Heat and mass transfer equations are examined in detail in the presence of heat source sink and Joule heating. Nonlinear mixed convection effect is examined. Disk is rotated with frequency Ω_1. B_0 is the strength of the magnetic field (see Fig. 1).

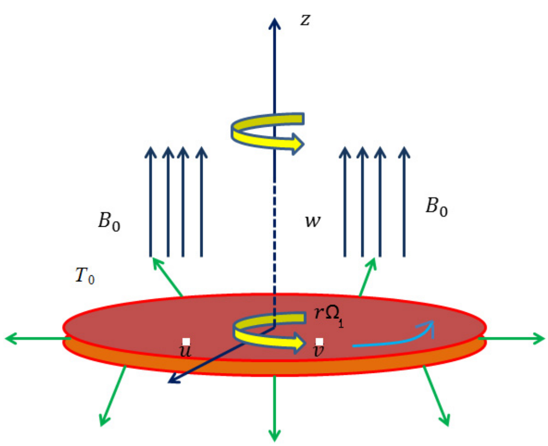

Fig. 1. (Color online) Schematic flow diagram.

Governing equations for present flow system are mentioned below[2]:

$$\frac{\partial u}{\partial r}+\frac{u}{r}+\frac{\partial w}{\partial z}=0, \tag{1}$$

$$u\frac{\partial u}{\partial r}+w\frac{\partial u}{\partial z}=\nu\frac{\partial^2 u}{\partial z^2}-\frac{\sigma B_0^2 u}{\rho}+g(\beta_1(T-T_\infty)+\beta_2(T-T_\infty)^2 + \beta_3(C-C_\infty)+\beta_4(C-C_\infty)^2), \tag{2}$$

$$\left.\begin{aligned}\left(u\frac{\partial T}{\partial r}+w\frac{\partial T}{\partial z}\right)&=\frac{k}{(\rho c_p)}\frac{\partial^2 T}{\partial z^2}+\tau D_B\left(\frac{\partial C}{\partial z}\frac{\partial T}{\partial z}\right)+\frac{\tau D_T}{T_\infty}\left(\frac{\partial T}{\partial z}\right)^2\\&\quad+\frac{Q_0(T_0-T_\infty)}{(\rho c_p)}\exp(-n\nu^{-0.5}\Omega^{0.5}z)+\frac{Q_l}{(\rho c_p)}(T-T_\infty)+\frac{\sigma B_0^2}{(\rho c_p)}u^2,\end{aligned}\right\} \tag{3}$$

$$u\frac{\partial C}{\partial r}+w\frac{\partial C}{\partial z}=D_B\frac{\partial^2 C}{\partial z^2}+\frac{D_T}{T_\infty}\left(\frac{\partial^2 T}{\partial z^2}\right)-k_r^2(C-C_\infty)\left(\frac{T}{T_\infty}\right)^{n_1}Exp\left[\frac{-E_a}{\kappa T}\right], \tag{4}$$

$$u\frac{\partial N}{\partial r}+w\frac{\partial N}{\partial z}=\frac{-bW_c}{\Delta C}\left(N\frac{\partial^2 C}{\partial y^2}+\frac{\partial C}{\partial z}\frac{\partial N}{\partial z}\right)+D_n\frac{\partial^2 N}{\partial z^2}, \tag{5}$$

with[2]

$$\left.\begin{aligned}&\mu\left.\frac{\partial u}{\partial z}\right|_{z=0}=\left.\frac{\partial \sigma}{\partial r}\right|_{z=0}=\left.\frac{\partial\sigma}{\partial T}\frac{\partial T}{\partial r}\right|_{z=0}-\left.\frac{\partial\sigma}{\partial C}\frac{\partial C}{\partial r}\right|_{z=0},\quad w=0,\quad T=T_0=T_\infty+Ar^2,\\&C=C_0=C_\infty+Br^2,\quad N=N_0 \text{ at } z=0\\&u\to 0,\quad T\to T_\infty,\quad C\to C_\infty,\quad N\to N_\infty,\quad \text{as } z\to\infty.\end{aligned}\right\}, \tag{6}$$

where surface tension is linear with concentration and temperature $\sigma=\sigma_0-\gamma_T(T-T_\infty)-\gamma_C(C-C_\infty)$ with $\gamma_T=-\frac{\partial\sigma}{\partial T}|_{T=T_\infty}$ and $\gamma_C=-\frac{\partial\sigma}{\partial C}|_{C=C_\infty}$.

Considering

$$\left.\begin{aligned}&u=r\Omega_1 f(\zeta),\ \zeta=y\sqrt{\frac{\Omega_1}{\nu}},\ w=\sqrt{\Omega_1\nu}H(\zeta),\ T=T_\infty+Ar^2\theta,\ C=C_\infty+Br^2\phi,\\&N=N_\infty+(N_0-N_\infty)\chi(\zeta).\end{aligned}\right\}. \tag{7}$$

After implementing the above transformations, we have

$$f''-f^2-hf'-Mf+\lambda\theta(1+\beta_t\theta)+\lambda N^*\phi(1+\beta_c\phi)=0, \tag{8}$$

$$\frac{1}{\Pr}\theta''-2f\theta+h\theta'+Q\exp(-n\zeta)+Ecf'^2+Q_t\theta+MEcf^2+Nt\theta'^2+Nb\theta'\phi'=0, \tag{9}$$

$$\frac{1}{Sc}\phi''-2f\phi+h\phi'+\frac{1}{Sc}\frac{Nt}{Nb}\theta''-k_1(1+\delta\theta)^{n_1}\exp\left(\frac{-E_1}{(1+\delta\theta)}\right)=0, \tag{10}$$

$$\chi'' - Pe[\phi''(\chi + \Omega) + \chi'\phi'] + Lb(f'\chi) = 0, \tag{11}$$

with

$$\left.\begin{matrix} f'(0) = -2Ma(1+r), \quad h(0) = 0, \quad \theta(0) = 1, \quad \phi(0) = 1, \quad \chi(0) = 1, \\ f(\infty) = 0, \quad \theta(\infty) = 0, \quad \phi(\infty) = 0, \quad \chi(\infty) = 0. \end{matrix}\right\}. \tag{12}$$

Parameters are mathematically addressed as

$$\left.\begin{aligned} & M = \frac{\sigma^* B_0^2}{\rho\Omega_1}, \quad \lambda = \frac{g\beta_1 A r^2}{r\Omega_1^2}, \quad \Pr = \frac{(\rho c_p)\nu}{k}, \\ & Ec = \frac{r^2\Omega_1^2}{(c_p)Ar^2}, \quad Q = \frac{Q_0}{\Omega_1(\rho c_p)}, \quad Q_t = \frac{Q_l}{\Omega_1(\rho c_p)} \\ & \beta_t = \frac{\beta_2 A r^2}{\beta_1}, \quad \beta_c = \frac{\beta_4 B r^2}{\beta_3}, \quad N^* = \frac{\beta_3 B r^2}{\beta_1 A r^2}, \\ & Ma = \frac{\gamma_T A}{\mu\Omega_1}\sqrt{\frac{\nu}{\Omega_1}}, \quad r = \frac{\gamma_C B}{\gamma_T A}, \quad \Omega = \frac{N_\infty}{N_w - N_\infty}, \\ & Nt = \frac{\tau D_T A r^2}{\nu T_\infty}, \quad Nb = \frac{\tau D_B B r^2}{\nu}, \quad k_1 = \frac{k_r^2}{\Omega_1}, \quad E_1 = \frac{E_a}{\kappa T_\infty}, \\ & Sc = \frac{\nu}{D_B}, \quad Pe = \frac{bW_c}{D_n}, \quad Lb = \frac{\nu}{D_n}. \end{aligned}\right\}. \tag{13}$$

3. Physical Interest

The physical interest like skin friction coefficient and heat transfer rate (Nusselt number) are addressed as

$$\left.\begin{aligned} Sh_x &= \frac{-r\frac{\partial C}{\partial z}}{Br^2}, \\ Nu_x &= \frac{-r\frac{\partial T}{\partial z}}{Ar^2}, \end{aligned}\right\}. \tag{14}$$

The dimensionless form is

$$\left.\begin{aligned} Sh_x \mathrm{Re}^{0.5} &= -\phi'(0), \\ Nu_x \mathrm{Re}^{-0.5} &= -\theta'(0). \end{aligned}\right\} \tag{15}$$

With $\mathrm{Re}_r = \frac{r^2\Omega_1}{\nu}$ is Reynolds number.

4. Convergence Analysis

By choosing suitable values of $\hbar_h$, $\hbar_f$, $\hbar_\theta$, $\hbar_\phi$ and $\hbar_\chi$ convergence of $h'(0)$, $f''(0)$, $\theta'(0)$, $\phi'(0)$ and $\chi'(0)$ is found. $\hbar$-curves at 16th order of approximation are drawn to find the suitable range for $h'(0), f''(0), \theta'(0), \phi'(0)$ and $\chi'(0)$. From Fig. 2, we found ranges of $\hbar$-curves as $-1.2 \le \hbar_h \le -0.3$, $-1.0 \le \hbar_f \le -0.2$, $-1.2 \le \hbar_\theta \le -0.4$, $-1.2 \le \hbar_\phi \le -0.8$ and $-1.1 \le \hbar_\chi \le -0.1$. By Table 1, we can see that $h'(0), f''(0), \theta'(0)$, $\phi'(0)$ and $\chi'(0)$ converges at 40th order of approximation.

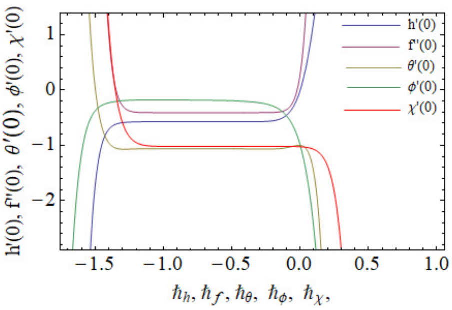

Fig. 2. (Color online) Combined h-curves.

Table 1. Convergence values for $h'(0)$, $f''(0)$, $\theta'(0)$, $\phi'(0)$ and $\chi'(0)$.

Order of approximation	$-h'(0)$	$-f''(0)$	$-\theta'(0)$	$-\phi'(0)$	$-\chi'(0)$
1	0.34441	0.4311	0.9888	0.57192	0.78254
8	0.57115	0.40887	1.06402	0.20061	0.86485
13	0.57123	0.40887	1.06301	0.18435	1.00121
14	0.57133	0.40887	1.06301	0.18295	1.00121
40	0.57133	0.40887	1.06301	0.17712	1.00121
50	0.57133	0.40887	1.06301	0.17712	1.00121
60	0.57133	0.40887	1.06301	0.17712	1.00121

5. Discussion

This section of paper is to elaborate the results of our research graphically. Figures 3–26 are sketched to analyze the important parameters impact against axial $(h(\zeta))$, radial velocities $(f(\zeta))$, temperature $(\theta(\zeta))$, motile microorganism profile $(\chi(\zeta))$, concentration profile $(\phi(\zeta))$, Nusselt number and Sherwood Impact of Marangoni number (Ma), Marangoni ratio parameter (r), magnetic parameter (M), mixed convection parameter (λ), nonlinear thermal and solutal mixed convection parameters (β_t) and (β_c), respectively versus axial and radial velocity is depicted in Figs. 3–8. Magnitude of axial and radial velocity profile rises for greater estimation of

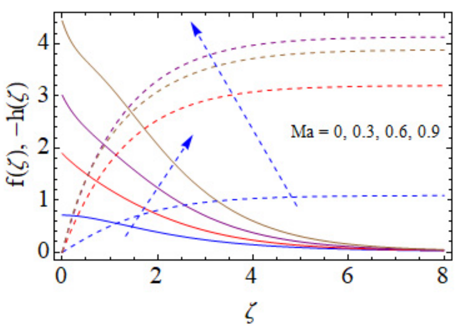

Fig. 3. (Color online) Ma on $(f(\zeta), -h(\zeta))$.

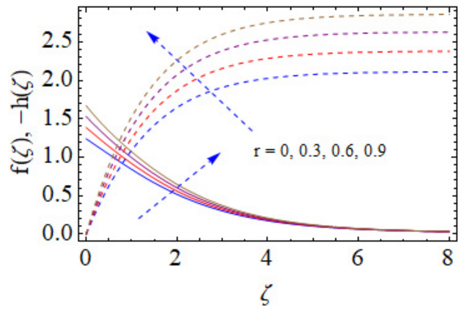

Fig. 4. (Color online) r on $(f(\zeta), -h(\zeta))$.

$(Ma = 0, 0.3, 0.6, 0.9)$ (see Fig. 3). Physically when Ma rises surface tension also starts increasing due to which velocity between the systems enhances. Figure 4 illustrates the influence Marangoni ratio parameter (r) against axial and radial velocity profiles. It shows also direct relation with velocities because in definition of r again γ_T is in direct relation due to which surface tension rises consequently velocity also enhances. Figure 5 displays the impact of magnetic parameter (M) against $(h(\zeta))$ and $(f(\zeta))$. Physically Lorentz force (resistive force) enhances due to the increment in M. That resistive force produces resistance for the flow particles hence velocity decay. Figure 6 shows the trend of $(h(\zeta))$ and $(f(\zeta))$ for higher values of mixed convection parameter (λ). Mixed convection is buoyancy forces to viscous forces. Due to increment in λ viscous forces are reducing that is why velocity enhances. Figures 7 and 8 are sketched to show the behavior of $(h(\zeta))$ and $(f(\zeta))$ against β_t and β_c. It is very interesting to see that axial and radial velocities are rising as we increase both the parameters (β_t, β_c).

Figures 9–15 are designed to show the results of temperature profile against Prandtl number (Pr), exponential dependent heat generation parameter (Q), Eckert number (Ec), thermal dependent heat source parameter (Q_t), thermophoretic parameter (Nt), ratio of Marangoni parameter (r) and Marangoni number (Ma). Figure 9 shows the effect of Prandtl number versus temperature profile. It is observed that temperature decays with increment in Pr. Physically thermal conductivity of

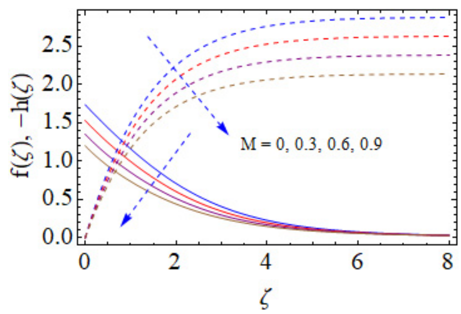

Fig. 5. (Color online) M on $(f(\zeta), -h(\zeta))$.

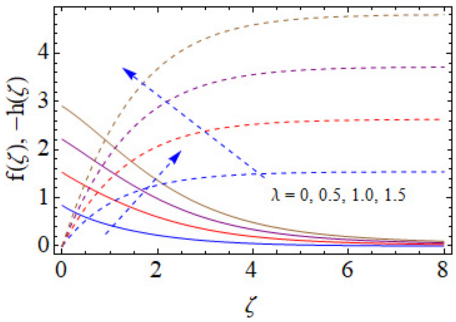

Fig. 6. (Color online) λ on $(f(\zeta), -h(\zeta))$.

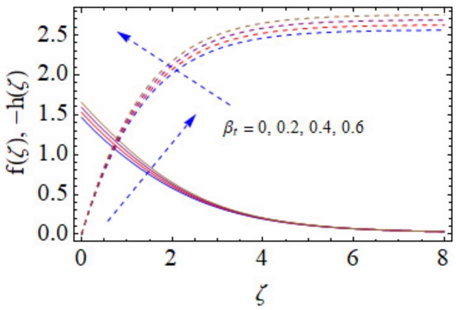

Fig. 7. (Color online) β_t on $(f(\zeta), -h(\zeta))$.

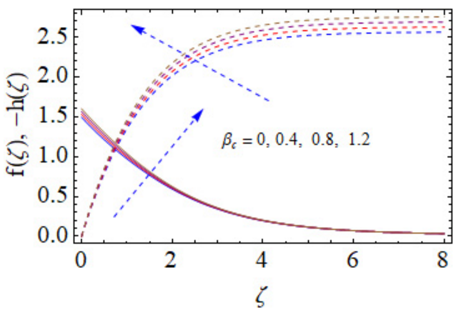

Fig. 8. (Color online) β_c on $(f(\zeta), -h(\zeta))$.

the fluid reduces with increase in Pr due to which θ decays. Figures 10 and 12 show the influence of (Q) and (Q_t) versus temperature profile. Physically with increase in (Q) and (Q_t) heat source provided to the system enhances due to which temperature rises. Figure 11 shows the trend of Eckert number via θ. By increasing values of Eckert number, total system of energy rises due to which temperature also rises. Figure 13 is about the behavior of Nt against temperature field. Physically, when we

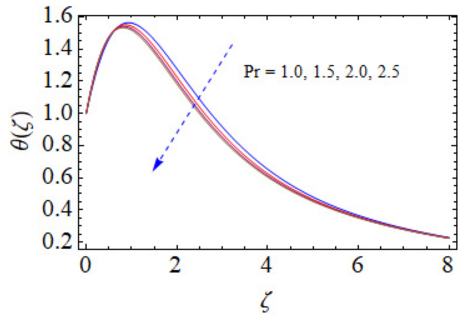

Fig. 9. (Color online) Pr on $\theta(\zeta)$.

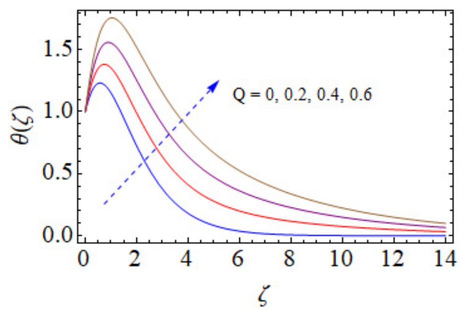

Fig. 10. (Color online) Q on $\theta(\zeta)$.

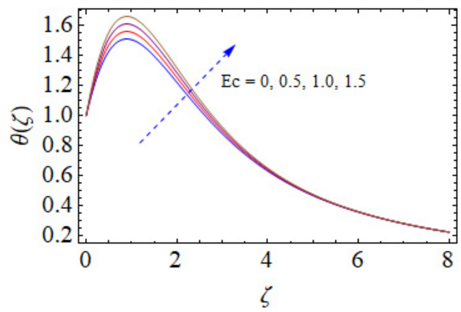

Fig. 11. (Color online) Ec on $\theta(\zeta)$.

increase the values of N_t thermophoretic force increases due to which hot particles move toward cold region, consequently temperature enhances. Figures 14 and 15 are about the impact of Marangoni number Ma and r versus temperature profile θ. By definition of Ma and r, we can see that both are increasing functions of surface tension. So, due to increase in surface tension, temperature rises for Ma and r.

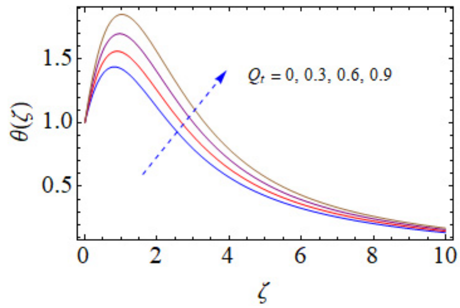

Fig. 12. (Color online) Q_t on $\theta(\zeta)$.

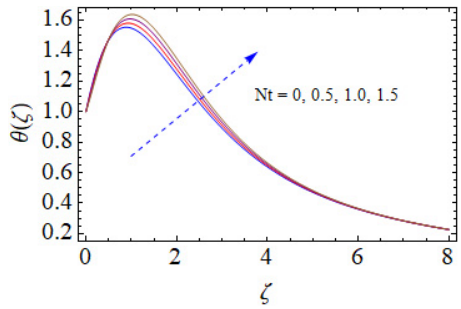

Fig. 13. (Color online) Nt on $\theta(\zeta)$.

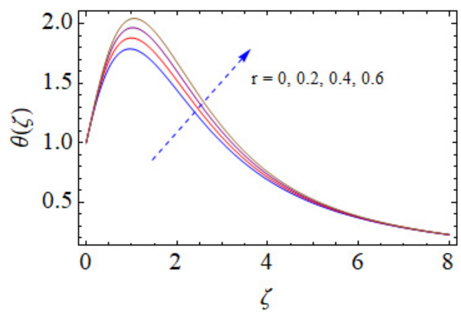

Fig. 14. (Color online) r on $\theta(\zeta)$.

Figures 16–18 are designed to elaborate the results of concentration profile via activation energy parameter (E_1), chemical reaction parameter (k_1) and Schmidt number (Sc). It is depicted that concentration profile rises for increasing values of (E_1) (see Fig. 16). With increase in values of activation energy parameter $\exp[\frac{-E_1}{1+\delta\theta}]$, Arrhenius function decays due to which productivity of chemical reaction decreases, hence, concentration decreases. For increasing values of chemical reaction parameter concentration of the fluid reduces (see Fig. 17). Figure 18 shows the impact of

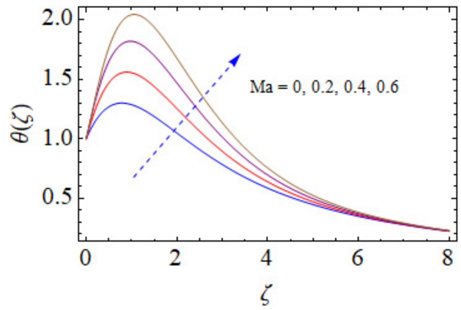

Fig. 15. (Color online) Ma on $\theta(\zeta)$.

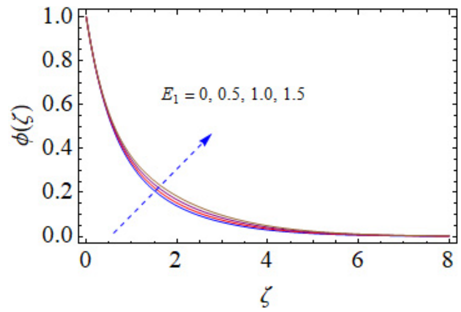

Fig. 16. (Color online) E_1 on $\phi(\zeta)$.

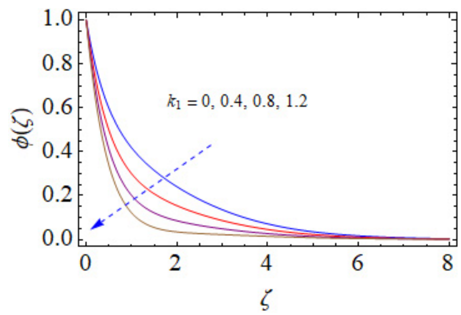

Fig. 17. (Color online) k_1 on $\phi(\zeta)$.

Schmidt number (Sc) against concentration profile. With increase in Sc, diffusivity of the fluid decays due to which ($\phi(\zeta)$) decays.

Figures 19–21 are associated with the behavior Peclet number (Pe), Schmidt number (Sc) and density difference parameter (Ω) against motile microorganism profile $\chi(\zeta)$. Figure 19 tells the influence of Pe against $\chi(\zeta)$. It is seen that $\chi(\zeta)$ decays for higher values of Pe. With increase in values of Pe, diffusivity of micro-organism decays hence $\chi(\zeta)$ decreases. Figure 20 depicts the impact of Sc on $\chi(\zeta)$.

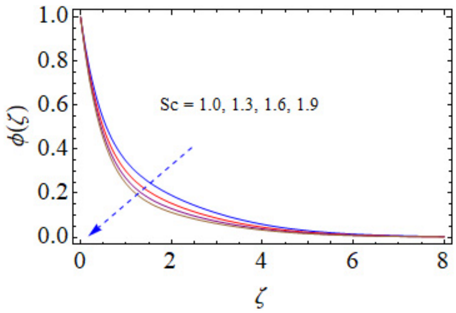

Fig. 18. (Color online) Sc on $\phi(\zeta)$.

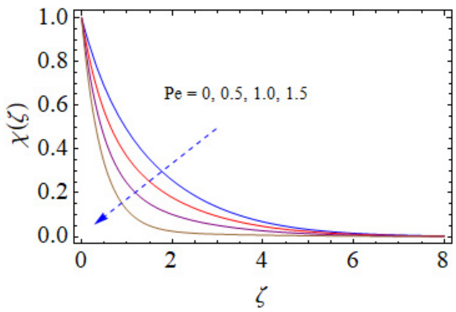

Fig. 19. (Color online) Pe on $\chi(\zeta)$.

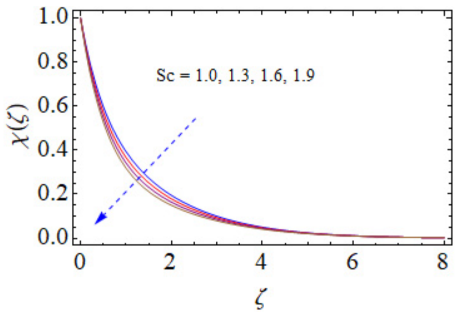

Fig. 20. (Color online) Sc on $\chi(\zeta)$.

While increment in values of Sc, motile microorganism density reduces. Figure 21 shows the trend of $\chi(\zeta)$ against Ω. With enhancement in values of Ω, density profile reduces because difference of density reduces for higher Ω.

Figures 22–25 are sketched to show the impact of Nusselt number and Sherwood number against pertinent parameters. Magnitude of Nusselt number rises with increase in ratio of Marangoni number (r) and thermal dependent heat source parameter (Q_t) (see Fig. 22) while opposite impact is seen against exponential

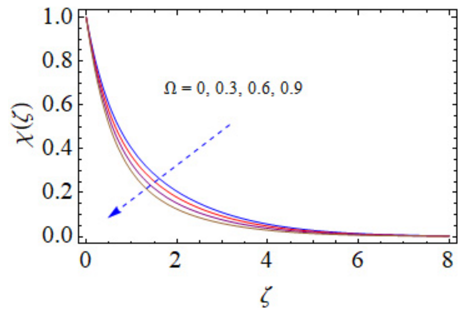

Fig. 21. (Color online) Ω on $\chi(\zeta)$.

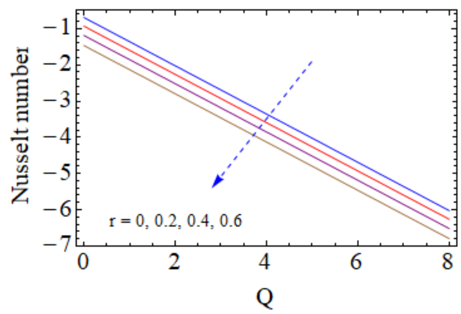

Fig. 22. (Color online) r and Q on Nusselt number.

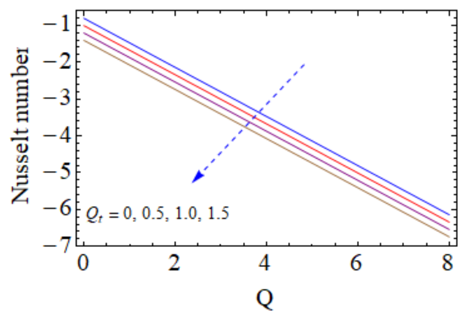

Fig. 23. (Color online) Q_t and Q on Nusselt number.

dependent heat source parameter (Q) (see Fig. 23) Figure 24 is about the impact of Brownian motion parameter (Nb) against Sherwood number. It is seen that Sherwood number enhances for larger Nb. Figure 25 shows that Sherwood number reduces with increase in activation energy parameter and thermophoretic parameter. Figure 26 is sketched to show the graphical validation of our result with Ref. 7. For nanoparticle volume fraction equals to zero in Ref. 7 we can see that in limiting case

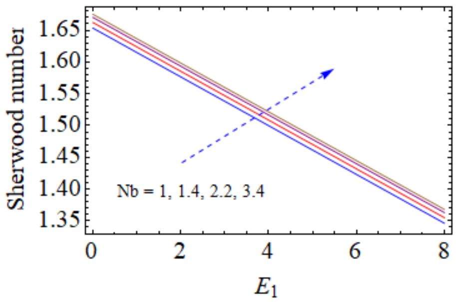

Fig. 24. (Color online) Nb and E_1 on Sherwood number.

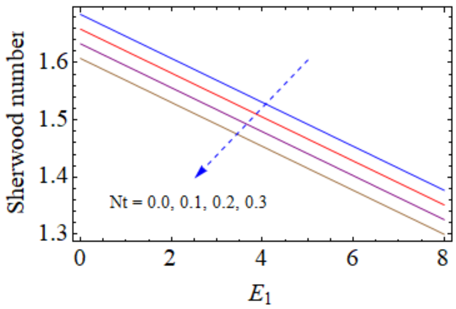

Fig. 25. (Color online) Nt and E_1 on Sherwood number.

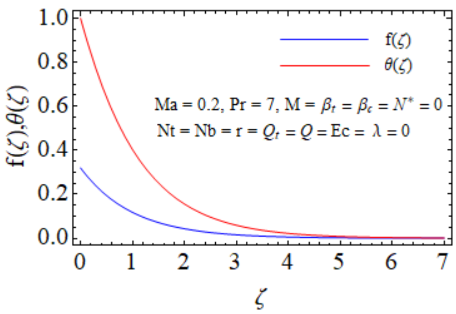

Fig. 26. (Color online) Comparison with Ref. 7 for Ma and Pr against $f(\zeta)$ and $\theta(\zeta)$.

we have found excellent agreement. We have drawn graph for velocity and temperature in Fig. 26 with all parameters equals to zero except Ma and Pr.

6. Conclusion

The keypoints of present analysis are shown below:

- It is seen that axial and radial velocities are increasing functions of Ma and r.
- h and f velocities are increasing via β_t and β_c.

- Temperature is increasing function of Ec, Ma and r.
- Concentration rises for higher activation energy parameter.
- Motile microorganism density profile reduces for higher Pe and Ω.

Acknowledgments

The research was supported by the National Natural Science Foundation of China (Grant Nos. 11971142, 11871202, 61673169, 11701176, 11626101, 11601485).

References

1. A. I. Mizev and A. I. Trofimenko, *Fluid Dyn.* **49**, 26 (2014).
2. B. Mahanthesh, B. J. Gireesha, N. S. Shashikumar, T. Hayat and A. Alsaedi, *Results Phys.* **9**, 78 (2018).
3. Y. Lin, L. Zheng and X. Zhang, *Mech Time-Depend Mater.* **19**, 519 (2015).
4. Y. Fujita, *Heat Transfer Enhancement of Heat Exchangers*, eds. S. Kakaç, A. E. Bergles, F. Mayinger and H. Yuncu (Kluwer, Dordrecht, The Netherlands, 1998), p. 325.
5. T. G. Roisman and P. Stephan, *J. Enhanced Heat Transf.* **10**, 369 (2003).
6. T. Gambaryan-Roisman and P. Stephan, *Therm. Sci. Eng.* **11**, 43 (2003).
7. Y. Lin and L. Zheng, *AIP Adv.* **5**, 107225 (2015).
8. J. Xu and A. Zebib, *J. Fluid Mech.* **364**, 187 (1998).
9. P. Colinet, J. C. Legros and M. G. Velarde, *Nonlinear Dynamics of Surface-Tension-Driven Instabilities* (Wiley, New York, 2001).
10. A. A. Nepomnyashchy, M. G. Velarde and P. Colinet, *Interfacial Phenomena and Convection* (Chapman and Hall, New York, 2001).
11. S. U. S. Choi, *ASME Int. Mech. Eng. Congress 231/MD* **66**, 99 (1995).
12. R. S. R. Gorla, S. M. M. El-Kabeir and A. M. Rashad, *J. Thermophys. Heat. Transf.* **25**, 183 (2011).
13. M. Fakour, A. Vahabzadeh and D. D. Ganji, *Propul. Power Res.* **4**, 50 (2015).
14. O. D. Makinde and A. Aziz, *Int. J. Therm. Sci.* **50**, 1326 (2011).
15. M. Mustafa, T. Hayat and S. Obaidat, *Int. J. Numer. Methods Heat Fluid Flow* **23**, 945 (2013).
16. M. A. A. Hamad, L. K. Mahny and M. R. Abdel-Salam, *Middle-East J. Sci. Res.* **8**, 764 (2011).
17. N. Bachok, A. Ishak and I. Pop, *ASME J. Heat. Transf.* **135**, 054501 (2013).
18. K. Zaimi, A. Ishak and I. Pop, *Sci. Rep.* **4** (2014) DOI:10.1038/srep04404.
19. F. Aman, A. Ishak and I. Pop, *Int. Commun. Heat. Mass Transf.* **47**, 68 (2013).
20. Md. J. Uddin, O. A. Bég, A. Aziz and A. I. Md Ismail, *Math. Probl. Eng.* **2015**, 621503 (2015).
21. M. J. Uddin, O. A. Bég and N. Amin, *J. Magn. Magn. Mater.* **368**, 252 (2014).
22. M. J. Uddin, O. A. Bég and A. I. Ismail, *J. Thermophys. Heat. Transf.* **29**, 513 (2015), 10.2514/1.T4372.
23. S. Uddin, M. Mohamad and M. Rahimi-Gorji, *Microsyst. Technol.* **26**, 405 (2020).
24. M. Kahshan, D. Lua and M. Rahimi-Gorji, *Int. J. Hydrogen Energy* **44**, 17041 (2019).
25. A. Hajizadeh, N. A. Shah, S. I. A. Shah, I. L. Animasaun, M. Rahimi-Gorji and I. M. Alarifi, *J. Mol. Liq.* **289**, 110964 (2019).
26. S. O. Adesanya, A. S. Onanaye, O. G. Adeyemi, M. Rahimi-Gorji and I. M. Alarifi, *J. Cleaner Prod.* **239**, 117608 (2019).
27. M. I. Khan, M. Waqas, T. Hayat and A. Alsaedi, *J. Colloid Interface Sci.* **498**, 85 (2017).

28. M. G. Reddy, M. S. Rani, K. G. Kumar, B. C. Prasannakumar and H. J. Lokesh, *Physica A Stat. Mech. Appl.* **551**, 123975 (2020).
29. M. Nazeer, F. Hussain, M. O. Ahmad, S. Saeed, M. I. Khan, S. Kadry and Y. M. Chu, *Surf. Interfaces* **22**, 100846 (2021).
30. M. G. Reddy, M. S. Rani, K. G. Kumar, B. C. Prasannakumar and A. J. Chamkha, *Physica A Stat. Mech. Appl.* **548**, 123991 (2020).
31. M. I. Khan, S. U. Khan, M. Jameel, Y. M. Chu, I. Tlili and S. Kadry, *Surf. Interfaces* **22**, 100849 (2021).
32. N. S. Shashikumar, B. C. Prasannakumara, M. Archana and B. J. Gireesha, *J. Nanofluids* **8**, 63 (2019).
33. M. Archana, M. G. Reddy, B. J. Gireesha, B. C. Prasannakumara and S. A. Shehzad, *Heat Transfer-Asian Res.* **47**, 957 (2018).